Cyril Fischer; Jiří Náprstek
Numerical solution of a stochastic model of a ball-type vibration absorber

Persistent URL: `http://dml.cz/dmlcz/703099`

NUMERICAL SOLUTION OF A STOCHASTIC MODEL OF A BALL-TYPE VIBRATION ABSORBER

Cyril Fischer, Jiří Náprstek

Institute of Theoretical and Applied Mechanics, AS CR, v.v.i.
Prosecká 76, Prague 9, Czech Republic
{fischerc,naprstek}@itam.cas.cz

Abstract: The mathematical model of a ball-type vibration absorber represents a non-linear differential system which includes non-holonomic constraints. When a random ambient excitation is taken into account, the system has to be treated as a stochastic deferential equation. Depending on the level of simplification, an analytical solution is not practicable and numerical solution procedures have to be applied. The contribution presents a simple stochastic analysis of a particular resonance effect which can negatively influence efficiency of the absorber.

Keywords: stochastic model, Monte Carlo method, stochastic Euler method, dynamical systems, non-holonomic system

MSC: 65C05, 65C20, 60G15, 37A50

1. Introduction

Ball-type passive tuned mass absorbers are popular means for reducing unwanted structural motion when a conventional pendulum-type device cannot be used. Contemporary lightweight structures are prone to vibration caused by traffic induced forces or natural ambient excitation. At the same time, new structures are often designed to exhibit their slenderness and installation of a classical absorber is not possible for aesthetic reasons. More compact ball-type absorbers are based on a free movement of a heavy ball of radius r which rolls inside a spherical cavity of radius $R > r$. In opposite to pendulum-based absorbers, damping of a ball movement can be adjusted to a prescribed value only with difficulties. Various techniques which implement additional damping into the absorber — as a rubber coating or liquid introduced in the cavity — entail a significant increase of maintenance costs. Consequently, insufficient damping makes the ball-type absorbers substantially more prone to objectionable effects stemming from a non-linear character of the system than are the pendulums. Thus, the design of the structure and the damping device has to be made so that the auto-parametric resonance states, occurrence of which

depends on system parameters and properties of possible excitation, are avoided for safety reasons.

The mathematical model of a ball pendulum represents a classical example of a simple non-holonomic system and, as such, it is regularly addressed from different points of view. The references date back to the beginning of 20th century, [14], up to recent publications, e.g., [3]. On the other hand, usage of the ball pendulum as a vibration absorber appears only recently, e.g., [8, 6]. Basic design guidelines of the ball-type absorber in a linearised 2D analogy and the practical implementation experience was reported on in [12]. Further analysis and stability assessment based on a non-linear 2D model was published later by the authors, [11]. The complete governing non-linear differential system derived using the Appell-Gibbs approach was used by the authors for numerical identification of the auto-parametric resonance effects in [9] and also for the stability analysis, [10]. It appeared that the auto-parametric resonance state is characterised by two forbidden regimes: spatial movement of the ball, when only an uni-directional excitation takes place, and multiple stable response regimes (solutions) for one set of excitation parameters. Occurrence of the both regimes is, however, limited to a narrow excitation frequency interval and/or large excitation amplitudes.

The experimental investigation of a ball pendulum was conducted by Pirner, [12]; the authors realized experiments with a spherical pendulum, [13]. The both experiments confirm appearance of the auto-parametric spatial response for deterministic harmonic excitation, however, the stability issues discussed in this work were not addressed. It appeared, however, that a behaviour of the ball pendulum and of the spherical pendulum are similar in many aspects. Although, to the best of the authors' knowledge, a stochastic analysis of the ball pendulum is still missing in the literature, there are several papers available which regard the stochastic analysis of spherical pendulums. Due to a non-linear nature of the problem, mostly the Monte Carlo simulation is used, see, e.g., [1] for an inverted pendulum case. More advanced approaches appear only rarely. For example, Viet Duc La, [5], use a stochastic linearisation technique which, however, requires a simplified problem. The rich literature regarding stochastic analysis of a general class of tuned mass dampers mostly limits its attention to damping efficiency maximization; the devices themselves are usually assumed only as planar or in a linearised form. Also studies where the behaviour of cranes with suspended payloads is modelled as a horizontally excited spherical pendulum, e.g., [7], do not concentrate to stability with respect to a random load.

The current work presents a basic stochastic analysis of the full 3D non-linear model of the ball-type absorber. Its aim is an assessment of a possibility to reach the spatial or multivalued response, characteristic for the auto-parametric resonance state, when narrow- or broadband stochastic excitation is assumed.

The paper is organized as follows. After this introduction, the non-linear model of the ball-type vibration absorber is shortly introduced. Its properties in the state of an auto-parametric resonance are described in Section 3. The analysis procedure and results are presented in Sections 4 and 5, respectively. Finally, Section 6 concludes.

2. Mathematical model

The governing differential systems used in this work is based on the Appell-Gibbs function, which is often referred to as an *energy acceleration function*:

$$S \;=\; \frac{1}{2}M(\ddot{u}_{Gx}^2 + \ddot{u}_{Gy}^2 + \ddot{u}_{Gz}^2) + \frac{1}{2}J(\dot{\omega}_x^2 + \dot{\omega}_y^2 + \dot{\omega}_z^2), \qquad (1)$$

where M – mass of the ball [kg], $J = 2/5Mr^2$ – central inertia moment of the homogeneous ball [kg m^2], $\omega_x, \omega_y, \omega_z$, – angular velocities of the ball with respect to its centre [rad s^{-1}], u_{Gx}, u_{Gy}, u_{Gz} – displacement of the ball centre with respect to absolute origin [m], u_{Cx}, u_{Cy}, u_{Cz} — displacement of the contact point [m].

Figure 1: Overview of the model

The Appell-Gibbs approach follows from the Gaussian fifth form of the basic principle of dynamics. It works with accelerations instead of velocities and in many cases it provides a simpler governing differential system than that obtained using a more common Lagrangian approach. The basic governing system is derived using the virtual-work principle and geometry relations and finally reads

$$
\begin{aligned}
J_s\rho\dot{\omega}_x &= (\quad (\ddot{u}_{Ay} + \rho(\omega_z\dot{u}_{Cx} - \omega_x\dot{u}_{Cz}))(u_{Cz} - R) - u_{Cy}(g + \rho(\omega_x\dot{u}_{Cy} - \omega_y\dot{u}_{Cx})))\\
J_s\rho\dot{\omega}_y &= (-(\ddot{u}_{Ax} + \rho(\omega_y\dot{u}_{Cz} - \omega_z\dot{u}_{Cy}))(u_{Cz} - R) + u_{Cx}(g + \rho(\omega_x\dot{u}_{Cy} - \omega_y\dot{u}_{Cx}))) \quad (2)\\
J_s\rho\dot{\omega}_z &= (\quad (\ddot{u}_{Ax} + \rho(\omega_y\dot{u}_{Cz} - \omega_z\dot{u}_{Cy}))u_{Cy} - (\ddot{u}_{Ay} + \rho(\omega_z\dot{u}_{Cx} - \omega_x\dot{u}_{Cz}))u_{Cx}) \;.
\end{aligned}
$$

where it was substituted: $J_s = \frac{(J + M\rho^2 R^2)}{M\rho^2}$ and $\rho = 1 - \frac{r}{R}$, and u_{Ax}, u_{Ay} denotes external kinematic excitation [m]. Additional non-holonomic constraints are based on the assumption of slippingless rolling of the ball in the cavity (see [9] for detailed derivation)

$$
\begin{aligned}
\dot{u}_{Cx} &= \omega_y(u_{Cz} - R) - \omega_z u_{Cy}\,,\\
\dot{u}_{Cy} &= \omega_z u_{Cx} - \omega_x(u_{Cz} - R)\,, \qquad\qquad (3)\\
\dot{u}_{Cz} &= \omega_x u_{Cy} - \omega_y u_{Cx}\,.
\end{aligned}
$$

3. Behaviour in the resonance

The resonance properties of the system given by Eqs. (2,3) are generally studied when the motion of the cavity, u_{Ax}, u_{Ay}, is prescribed as one harmonic component:

$$\ddot{u}_{Ax} = u_0\,\omega^2 \sin\omega t\,, \qquad \ddot{u}_{Ay} = 0\,. \qquad (4)$$

When varying the excitation frequency, the maximal response amplitude of the settled response in the state of resonance may attain different values for a single excitation frequency. Also the transverse component of the response may become non-negligible; its non-zero values represent spatial motion of the ball. The both effects are directly related to an auto-parametric resonance, which emerges due to a non-linear connection between two principal directions of the movement.
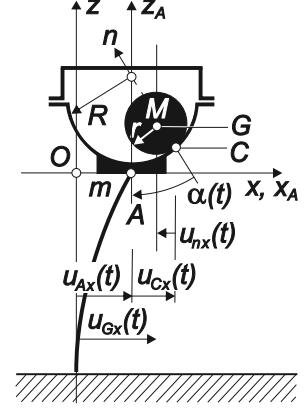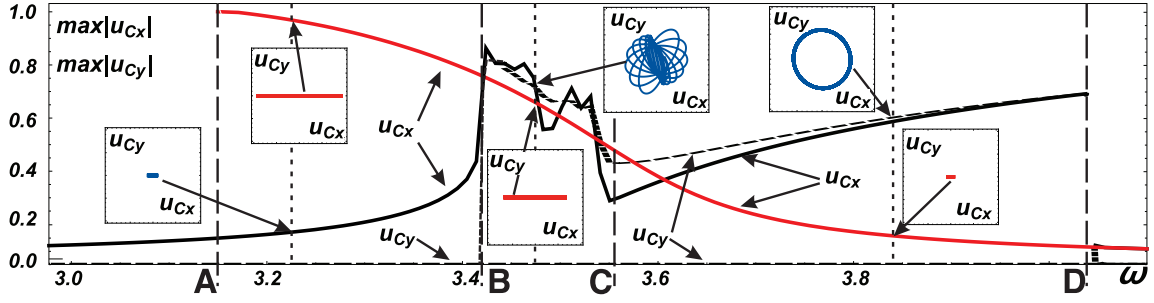
Figure 2: Resonance plots for prescribed harmonic movement in x direction, Eq. (4). Maximal amplitudes of the settled response reached for a given excitation frequency are shown on the vertical axis. Longitudinal amplitude: solid, transversal amplitude: dashed. Insets show projections of the trajectory for three particular frequencies.

The situation is illustrated in Fig. 2. The resonance area — the interval between points A and D — is characterised by an overlapped resonance curve. Two levels of the planar response are present between A–B, planar, chaotic or multiperiodic response exists in the interval between B–C, planar or elliptic response appears between C–D. As it was presented by the authors in [10], the individual branches differ also in terms of stability with respect to perturbation of the respective settled solutions. The upper branch in interval A–B is planar (i.e., $u_{Cy} = 0$) and is sensitive to any perturbation in the transverse direction. On the other hand, the circular motion in interval C–D is stable with respect to perturbation in any direction in the beginning of the interval, its stability gradually decreases with increasing excitation frequency ω.

The stability of the individual response branches may be measured by a size of the respective basin of attraction (BA). While the BA of the upper branch in interval A–B forms a rank-2 set (u_{Cx}, ω_y) in the complete 5-dimensional parameter space $(u_{Cx}, u_{Cy}, \omega_x, \omega_y, \omega_y)$, see [10] for details, in interval C–D the BA of the upper branch fills a full-rank subset of the parameter space. Its volume decreases as the excitation frequency increases. Thus, the access to the upper branch from general initial conditions is becoming increasingly difficult for higher excitation frequencies.

The present analysis is targeted to the stability analysis of the upper (elliptic) branch in the C–D interval with respect to stochastic excitation.

4. Random response analysis

The stationary random load is usually described by a spectral density matrix and an underlining probability distribution (preferably Gaussian). The stationarity assumption represents an acceptable simplification in this analysis.

As an example of the spectral density, which is frequently used in engineering applications corresponding to wind effects, servers the so-called Davenport's spectrum, [2], which represents the cross-spectrum of horizontal gustiness in two points x_1, x_2 near the ground in high winds. It represents a narrow-band random

process. On the other hand, the peak of the auto-parametric resonance of the ball absorber is also quite narrow, cf. Fig. 2 and [10]. For this reason, two different random input processes were taken into account: (i) a broadband approximation of the white noise process, and (ii) a narrow-band process, spectral density of which is concentrated in the resonance interval of the absorber. The former case of a purely random excitation was used for assessment of the possibility of emergence of the high-energy spatial response due to an ambient broadband noise. The latter case was selected to assess stability of the spatial response with respect to random perturbations. In this latter case, two excitation variants were used, namely a harmonic movement perturbed by a band-limited Gaussian noise with spectrum concentrated around the harmonic movement frequency, $\xi_1(t)$, and a pure band-limited Gaussian noise with a similar spectral density and greater intensity, $\xi_2(t)$.

$$(a) \quad \ddot{u}_{Ax1} = \xi_1(t) + u_0\omega^2 \sin\omega t\,, \qquad (b) \quad \ddot{u}_{Ax2} = \xi_2(t)\,. \tag{5}$$

Processes ξ_j, $j = 1, 2$ $[\mathrm{m\,s^{-2}}]$ in the both variants were scaled to deliver an approximately equal energy to the model. To keep continuity of realizations $\ddot{u}_{Axj}$, random processes ξ_j are modelled in the form of

$$\xi_j = \sqrt{\frac{\Delta t}{T}} \sum_{i=1}^{M} u_{j,i} w_{j,i}^2 \sin(w_{j,i}t)\,, \qquad j = 1, 2\,, \tag{6}$$

where Δt is the time step used during integration [s], $T = M\,\Delta t$ is the total integration time [s] and $u_{j,i}, w_{j,i}$ are normally distributed random variables representing amplitude [m] and frequency $[\mathrm{rad\,s^{-1}}]$, respectively; $u_{j,i} \in N(0, \sigma_{u_j})$, $w_{j,i} \in N(\omega, \sigma_{\omega_j})$. Relation (6) represents a continuous variant of the traditional algorithm due to Shinozuka [15], which is originally based on FFT.

Two numerical methods were used for different random excitation processes. The modified stochastic Euler method (Itô version), [4], was used for the white noise excitation. This method uses a fixed step length, which can be problematic with respect to integration accuracy, when the step is too long, and also to stochastic properties of the response, if the step is too small. On the other hand, the Euler algorithm is simple and convenient for parallelization, e.g., using GPU. In the case of the band-limited excitation, the Monte Carlo simulation was used. The equations of motion were repeatedly integrated using the second Gear's method in an implementation of the `NDSolve` function in Wolfram Mathematica. This method encompasses advanced features as accuracy checking and thus it assures credible results even for long simulation times.

When dealing with non-linear models, the results of simulation are generally not Gaussian even for normally distributed inputs. This applies also to this case and, consequently, the results have to be represented by an estimate of a (time dependent) probability distribution. Histograms are used for this purpose in the this work.

The movement of the ball may exhibit a very complicated trajectory, namely when the chaotic or multi-periodic response occurs in interval B–C. The elliptical

spatial response, on the other hand, is periodic and intersects the coordinate axes always in the same points. When random excitation is assumed, the trajectory deviates from an ideal ellipse depending on variance of the random process. The presented histograms count values of the both spatial variables at the moments when the trajectory intersects the respective axes, i.e., values $|u_{Cx}(t_x)|, |u_{Cy}(t_y)|$, where $u_{Cx}(t_y) = 0$, $u_{Cy}(t_x) = 0$ and $t_x, t_y > t_0$; the time threshold $t_0 > 0$ is introduced to pass over interval $(0, t_0)$ of the transient response. For deterministic excitation, the histograms will be concentrated in values corresponding to intersection points of the elliptic trajectory and both axes. When random perturbation of the harmonic input increases, the centre of gravity of the histogram becomes blurred. A further increase in the random perturbation intensity may cause a change of the type of the response and a jump to the lower solution branch, which is characterised by a negligible value of the transversal component and a small but non-zero value of the longitudinal component.

5. Results

5.1. White noise excitation

The first test checks a possibility of the spherical absorber to enter the state of a spatial response, i.e., that with non-zero amplitudes in the transversal direction u_{Cy}. In the case of deterministic harmonic excitation and non-zero but negligible initial conditions, the response state corresponding to the spatial branch of the resonance curve in the C–D interval is not accessible.

It appears that in the case of broad-band white-noise excitation the spatial response may emerge depending on the variance of the input random process. This result follows from Fig. 3 which shows probability density estimates for components $u_{Cx}|_{y=0}$ and $u_{Cy}|_{x=0}$ for an increasing white noise intensity; each simulation begins from "small" initial conditions $u_{Cx}(0) = u_{Cy}(0) = 0.01$ and counts axes crossings for the both components in time interval $t \in (400, 600)$. Starting from the white noise intensity $\sigma = 0.15$, the transversal component becomes positive and for $\sigma \geq 0.35$ is the random response almost symmetric in the both components. However, the elliptic periodic response, which is typical for the upper spatial branch in the interval C–D, does not appear dominant in any histogram.

The random simulation was performed using the modified stochastic Euler method with $\Delta t = 2^{-6}$. The computation was restarted 240 times. Approximately 100 axes crossings were counted in each simulation for $t \in (400, 600)$, which number gives in total ca. 2.4×10^5 samples for each histogram.

5.2. Stability of the spatial movement

Stability of the periodic spatial movement was assessed using two slightly different approaches. Firstly, a harmonic excitation with frequency corresponding to the periodic spatial response was applied together with a band-limited random noise, $\ddot{u}_{Ax1}$, Eq. (5a). Secondly, a purely random process was considered with band-limited
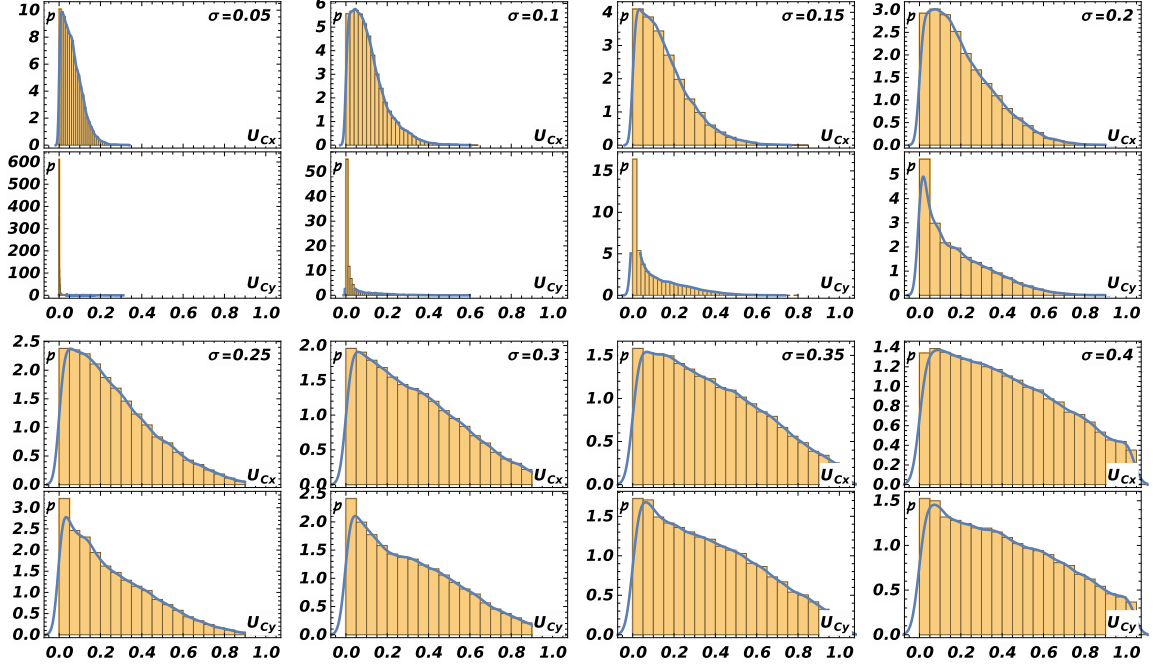
Figure 3: The probability density estimates for components $u_{Cx}|_{y=0}$ and $u_{Cy}|_{x=0}$ for $t \in (400, 600)$ and increasing white noise intensity σ, starting from "small" initial conditions $u_{Cx}(0) = u_{Cy}(0) = 0.01$, $\sigma_\omega = 0.5$, $\sigma_u = 0.02$, $M = 240, 10^5$ realizations.

spectral density concentrated around the corresponding harmonic frequency, $\ddot{u}_{Ax2}$, Eq. (5b). The both load cases resulted in random processes which were comparable in terms of the spectral density and variance. The results were also similar to each other. Thus, only results regarding the first case are presented.

Figure 4 shows changes in the response histograms for selected resonance frequencies from the interval C–D in rows, the individual columns correspond to different time instants in the simulation course $t = 200, 400, 600, 800$ for 10^5 realizations. The first row in Fig. 4 indicates that for $\omega = 3$ the response is spatial, the maximal values of histograms correspond to the deterministic periodic trajectory, however, the variance of the response is high. Moreover, the profile of histograms does not change significantly for increasing simulation time t. This fact indicates a high stability of the spatial movement at the lower end of the resonance interval C–D.

The second and third rows in Fig. 4 shows, for $\omega = 4$ and 5, two significant peaks in the histograms for $t = 200$; the upper ones (for values 0.8 and 0.9, respectively) correspond to the deterministic periodic trajectories. It seems that the lower peaks reflect gradual convergence to the lower planar response, because they shift towards the theoretical values for an increasing simulation time.
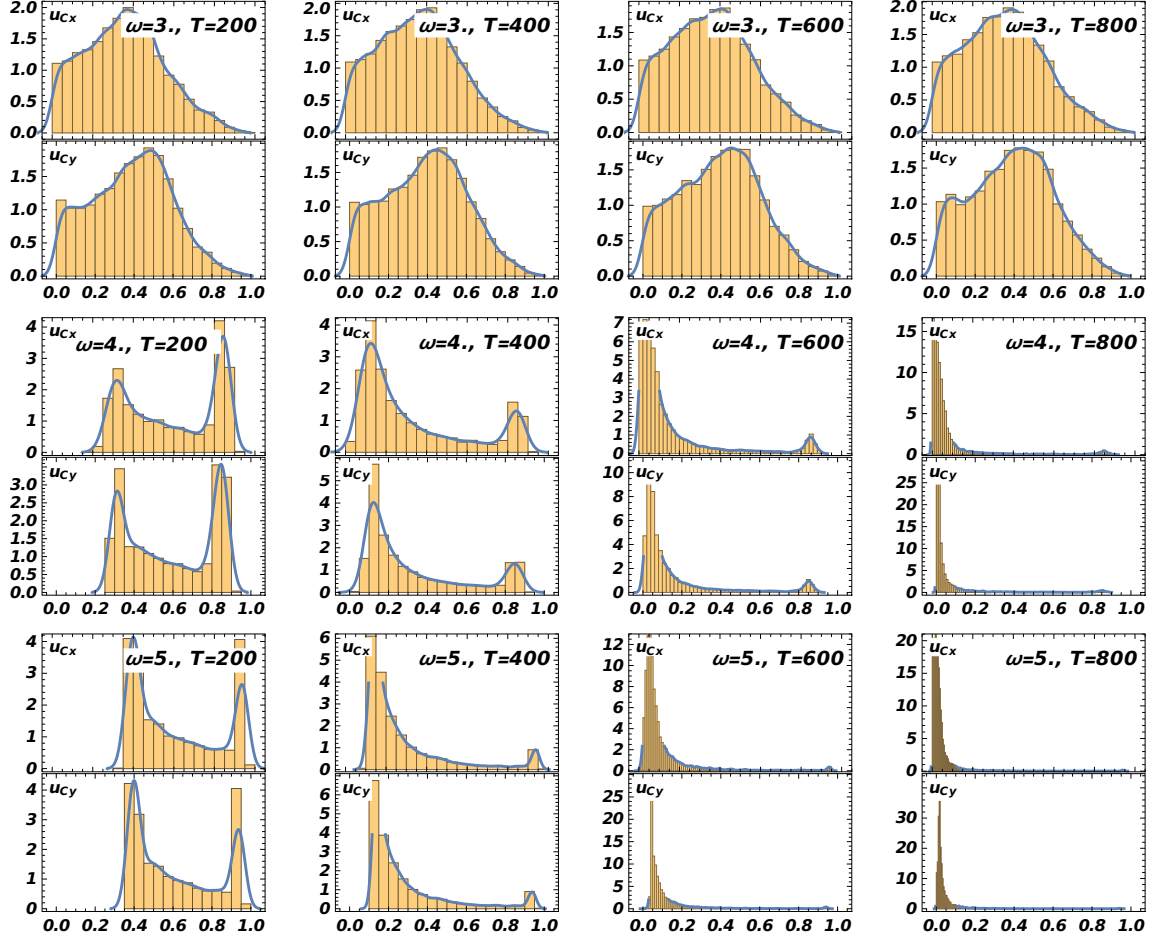
Figure 4: The probability density estimates for components $u_{Cx}|_{y=0}$ and $u_{Cy}|_{x=0}$ for $\omega = 3, 4, 5 \text{ rad s}^{-1}$, and varying duration of random excitation, $T = 200, \ldots, 800 \text{ s}$, $\sigma_\omega = 0.5$, $\sigma_u = 0.02$, $M = 240$, 10^5 realizations.

6. Conclusions

The ball-type passive tuned mass vibration absorber is an efficient damping device which proved very well being used at slender structures exposed to wind excitation. However, these devices are generally designed using a simplified 2D model derived according to needs of the structural engineer. The device is supposed to work in linear mode which neglects any type of the auto-parametric resonance effects. Due to a relatively low structural damping, the absorber is theoretically prone to a stability loss in a very particular loading case, i.e., when the load frequency coincide with the narrow interval of the auto-parametric resonance.

The current work, however, revealed that the spatial response of the absorber can emerge also due to a broadband random excitation, provided that the intensity of the random noise exceeds certain limit. It was also shown that the periodic spatial movement of the ball within the absorber is unfavourably stable with respect

47

to band-limited random perturbations that correlate with the respective resonance frequency.

The both results indicate a need for further investigation of the topic. A more thorough parameter study should comprise different system parameters (e.g., damping values), longer integration times, selection of different integration step lengths, etc. However, it can be concluded that occurrence of the auto-parametric effects in practice is more probable than it was expected. This can be dangerous for structures if adequate countermeasures are not applied.

References

[1] Bar-Avi, P. and Benaroya, H.: Non-linear dynamics of an articulated tower in the ocean. Journal of Sound and Vibration **190** (1996), 77–103.

[2] Davenport, A.G.: The spectrum of horizontal gustiness near the ground in high winds. Quarterly Journal of the Royal Meteorological Society **87** (1961), 194–211.

[3] Hedrih, K.: Rolling heavy ball over the sphere in real Rn3 space. Nonlinear Dynamics **97** (2019), 63–82.

[4] Kloeden, P. and Platen, E.: *Numerical Solution of Stochastic Differential Equations.* Springer, Berlin-Heidelberg, 1992.

[5] La, V.D.: Combination of partial stochastic linearization and Karhunen-Loeve expansion to design Coriolis dynamic vibration absorber. Mathematical Problems in Engineering **2017** (2017), 1–11.

[6] Legeza, V., Dychka, I., Hadyniak, R., and Oleshchenko, L.: Mathematical model of the dynamics in a one nonholonomic vibration protection system. International Journal of Intelligent Systems and Applications **10** (2018), 20–26.

[7] Litak, G., Margielewicz, J., Gaska, D., Yurchenko, D., and Dabek, K.: Dynamic response of the spherical pendulum subjected to horizontal Lissajous excitation. Nonlinear Dynamics **102** (2020), 2125–2142.

[8] Matta, E., De Stefano, A., and Spencer Jr., B.F.: A new passive rolling-pendulum vibration absorber using a non-axial guide to achieve bidirectional tuning. Earthquake Engineering and Structural Dynamics **38** (2009), 1729–1750.

[9] Náprstek, J. and Fischer, C.: Limit trajectories in a non-holonomic system of a ball moving inside a spherical cavity. Journal of Vibration Engineering & Technologies **8** (2020), 269–284.

[10] Náprstek, J. and Fischer, C.: Stable and unstable solutions in auto-parametric resonance zone of a non-holonomic system. Nonlinear Dynamics **99** (2020), 299–312.

[11] Náprstek, J., Fischer, C., Pirner, M., and Fischer, O.: Non-linear model of a ball vibration absorber. In: M. Papadrakakis, M. Fragiadakis, and V. Plevris (Eds.), *Computational Methods in Applied Sciences*, vol. 2, pp. 381–396. Springer Netherlands, Dordrecht, 2013.

[12] Pirner, M. and Fischer, O.: The development of a ball vibration absorber for the use on towers. Journal of the International Association for Shell and Spatial Structures **41** (2000), 91–99.

[13] Pospíšil, S., Fischer, C., and Náprstek, J.: Experimental analysis of the influence of damping on the resonance behavior of a spherical pendulum. Nonlinear Dynamics **78** (2014), 371–390.

[14] Routh, E.: *Dynamics of a system of rigid bodies*. Dover Publications, New York, 1905.

[15] Shinozuka, M. and Jan, C.M.: Digital simulation of random processes and its applications. Journal of Sound and Vibration **25** (1972), 111–128.